archives
of thermodynamics
Vol. **40**(2019), No. 2, 107–135
DOI: 10.24425/ather.2019.129544

Second law optimization and parametric study of a solar air heater having artificially roughened absorber plate

MUKESH KUMAR SAHU
RADHA KRISHNA PRASAD*

Department of Mechanical Engineering, National Institute of Technology, Jamshedpur, Jharkhand, India, Pin-831014

Abstract In present article a mathematical model of arc shape wire roughened solar air heater, on the basis of energy and exergy output rates, entropy generation rate and augmentation entropy generation number, has been developed. A parametric study leading to entropy generation minimization has also been performed. In the analysis the geometric and operating parameters which have been considered as variable are: inlet air temperature, duct depth, collector width to duct depth ratio, mass flow rate per unit collector area, and temperature rise parameter . Results have been presented to see the effects of these values on the energy and exergy output rates of the roughened solar air heater. Effect of different values of wire rib roughness parameters on entropy generation has also been presented. Finally, design curves and optimization for different rib roughness parameters on the basis of minimum entropy generation number with temperature rise parameter, have been presented and optimum values also have been found out 0.004 to 0.010 $(Km^2)/W$. The entropy generation rate obtained for the system, in the present work has been compared with those obtained for solar air heater with different roughness geometries on absorber plates available in the literature for common roughness parameters and operating parameters which validate the present results.

Keywords: Artificial roughness; Entropy generation; Entropy generation minimization; Augmentation entropy generation number; Solar air heater

*Corresponding Author. Email: rkprasad.me@nitjsr.ac.in

Nomenclature

A_c	–	surface area of absorber plate, m^2
C_p	–	specific heat of air, J/kg K
D	–	hydraulic diameter of solar air heater duct, m
e	–	rib roughness height, m
G	–	mass flow rate per unit collector area kg/s m^2
g	–	gravitational acceleration, m/s^2
h	–	heat transfer coefficient, W/m^2K
h_e	–	equivalent heat transfer coefficient, W/m^2 K
h_{c-ab-f}	–	convective heat transfer coefficient between air and absorber plate, W/m^2 K
h_{c-bp-f}	–	convective heat transfer coefficient between air and bottom plate, W/m^2 K
$h_{r-ab-bp}$	–	radiative heat transfer coefficient between absorber plate and bottom plate, W/m^2 K
H	–	depth of solar air heater duct, m
I	–	intensity of global solar radiation, W/m^2
K_a	–	thermal conductivity of air, W/m K
K_g	–	thermal conductivity of glass cover, W/m K
K_i	–	thermal conductivity of insulation, W/m K
L	–	length of solar air heater duct, m
L_1	–	spacing between glass cover and absorber plate, m
L_g	–	thickness of glass cover, m
M	–	number of glass covers
$\dot{m}$	–	mass flow rate of air, kg/s
Na	–	entropy generation number
P	–	roughness pitch, m
p_a	–	atmospheric pressure, N/m^2
$\triangle p$	–	pressure drop across the duct, N/m^2
Q_u	–	useful heat gain, W
SAH	–	solar air heater
T_g	–	cover glass temperature, K
T_{fo}	–	outlet air temperature, K
T_s	–	sky temperature, K
T_{fi}	–	air inlet temperature, K
T_{pm}	–	mean absorber plate temperature, K
T_{fm}	–	mean air temperature in the duct, K
T_{bm}	–	mean bottom plate temperature, K
t_e	–	thickness of collector edge, m
$\frac{\triangle T}{I}$	–	air temperature rise parameter $\left(=\frac{(T_{fo}-T_{fi})}{I}\right)$, Km^2/W
U_L	–	overall heat loss coefficient, W/m^2K
U_b	–	bottom loss coefficient, W/m^2K
U_s	–	side loss coefficient, W/m^2K
U_t	–	top loss coefficient, W/m^2K

V – air velocity through the duct, m/s
V_w – wind velocity, m/s
W – width of solar air heater duct, m
$\dot{W}p$ – pumping or mechanical power, W

Greek symbols

μ – absolute viscosity of air, N s/m^2
$(\tau\alpha_a)_e$ – effective transmittance-absorptance product
ρ_a – density of air, kg/m^3
α – angle of attack, degree
ϕ – chamfered angle, degree
α_a – absorptivity of absorber plate
$\alpha/90$ – flow-attack-angle
δ_i – insulation thickness, m
σ – Stefan-Boltzman constant, W/m^2 K^4
ε_b – emissivity of bottom plate
ε_a – emissivity of absorber plate
ε_g – emissivity of glass cover
β – tilt angle of collector surface, degree
η_{th} – thermal efficiency
ν – kinematic viscosity of air, m^2/s

Dimensionless parameters

e/D – rib height-to-duct hydraulic diameter ratio
f – friction factor
F_R – collector heat-removal factor
F' – collector efficiency factor
Nu – Nusselt number
Pr – Prandtl number
P/e – rib pitch-to-height ratio
Re$^+$ – roughness Reynolds number
Ra – Rayleigh number
g/e – relative gap width
d/w – relative gap position
Gr – Grashof number
l/s – relative length of grid
Re – Reynolds number
St – Stanton number
W/H – aspect ratio of collector duct

1 Introduction

Solar air heater (SAH) is a special type of heat exchanger that converts the solar radiation energy into useful thermal energy and transfers the same to air passing through it [1]. The conventional SAH has low efficiency due to poor convective heat transfer coefficient between main heated wall (absorber plate) and air flowing through it [2,3]. Sahu and Prasad [4] carried out an investigation on optimal thermohydraulic performance of a SAH having arc-shaped wire rib roughness and developed correlations between roughness parameters and operating parameters that leads to optimum effective efficiency. Gawande *et al.* [5] presented a detailed review on the application of different types and geometries of roughness on the absorber plate for enhancement in the heat transfer rate of simple SAH. Singh *et al.* have done their analytical investigations on second law of thermodynamics based exergy efficiency of discrete V-down wire rib roughness geometry on absorber plate of SAH [6]. Chamoli and Thakur presented the exergy based evaluation of SAH having V-down perforated baffles on the absorber plate of air heater duct and optimized the results [7]. Kaz/'e and Tchinda carried out an exergetic analysis of three types of SAHs viz. downward flat plate collector, unglazed selective absorber collector and artificially roughened absorber surface collector [8]. Exergy analysis and entropy generation analysis (EGA) are powerful tools that have been successfully applied by various researchers in the design [9–11], optimization, economic evaluation and performance evaluation of different thermal energy systems. Bejan analysed entropy generation in fundamental convective heat transfer for the four different flow configurations [12]: pipe flow, flow over flat plate, flow through single cylinder and in smooth rectangular duct. Bejan also investigated the concept of irreversibility or exergy destruction for heat exchanger design [13]. He presented a useful design approach for a heat exchanger by employing the thermodynamics based second law analysis. Nag and Mukherjee have done their analysis on thermodynamic optimization for a duct subjected to constant temperature [14]. They concluded that the initial temperature difference between fluid and the heated wall is a chief design criterion. Ko and Ting analyzed entropy generation (EG) by laminar forced convection in a curved rectangular shaped duct [15]. They investigated the optimal design conditions based on the minimal entropy generation or least irreversibility generation in the flow. Ko numerically analyzed the entropy generation number and obtained the optimal Reynolds number for double-sine shape ducts with variations in the values of aspect

ratio [16]. Yilbas *et al.* investigated on second law analysis for the circular shape duct with restriction [17], while Altfeld and Leiner carried out second law optimization for the flat-plate solar air heaters [18]. Sahiti *et al.* experimentally investigated the heat transfer and pressure drop characteristics of a double-pipe pin fin heat exchanger and optimized the results on the basis of entropy generation minimization for different duct flow-lengths and different pin lengths [19]. Bejan presented the methods of exergy analysis and entropy generation minimization for different thermal systems [20]. Ratts and Raut applied entropy generation minimization (EGM) method to optimize a thermal system [21]. They obtained an optimal Reynolds number for laminar and turbulent flows and compared optimal Reynolds number with minimum entropy generation for square, equilateral triangle and rectangle cross-sectional ducts aspect ratios of 2 and 8. Zhou *et al.* developed an optimization model for plate-fin heat exchangers based on the entropy generation minimization method [22]. They employed specific entropy generation rate for optimization, considering the total heat transfer area of a plate-pin fin heat exchanger as a constraint. Layek *et al.* have carried out investigations on second law optimization of a SAH having chamfered grooved roughness on absorber plate [23].

From the above literature review it is found that the analyses on exergy efficiency, entropy generation minimization and thermodynamic or second law based optimization have been carried out by the researchers to optimize different thermal systems including SAHs. To the best of our knowledge, a few investigations have been performed on entropy generation minimization, optimization and parametric study of rib roughened SAH together, which necessitates more work in this area to be carried out. The objective of the present work is to develop a mathematical model to evaluate the energy and exergy output rates of a SAH having arc shape wire roughness geometry on its absorber plate at air flow side. The efficient conversion of solar energy into useful energy is a primary objective in design of any solar energy system, which can also be achieved by minimization of the entropy generation in thermodynamic processes of the system. In view of this, second law analysis has been carried out to obtain an optimal thermodynamic design of the system which minimizes the entropy generation rate. Finally, design curves with geometrical and operating conditions leading to the minimum entropy generation rate have been presented to study the effects of the different parameters.

2 Theoretical analysis

2.1 Analysis of solar energy collector

Figure 1 shows the schematic view of the solar air heater duct having a simple flat plate as absorber. The collector is having a single glass cover of 5 mm thickness on the top to reduce the top heat loss and is having insulation of sufficient thickness on its other three sides to reduce bottom and side losses. The absorber plate, two parallel wooden sides and the bottom plate form a passage to make the air to flow between absorber plate and bottom plate of the collector duct.

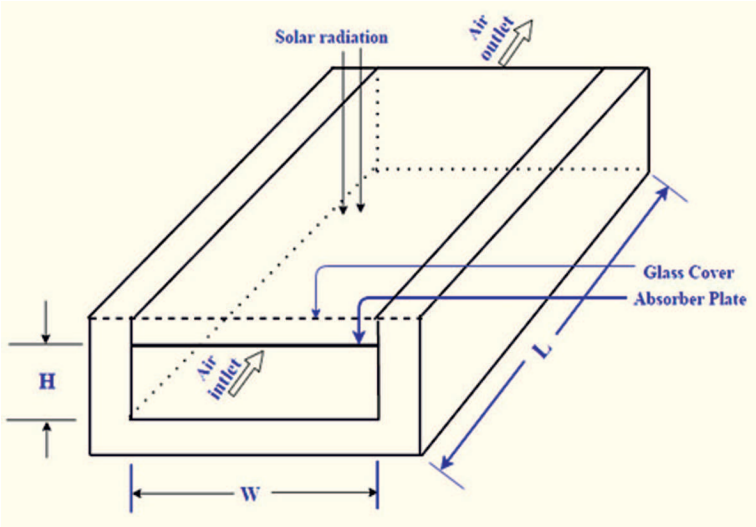

Figure 1: Solar air heater duct with simple absorber plate.

Figure 2 shows the geometry of arc shape wire rib roughness on absorber plate. In both SAHs air is flowing below the absorber plate. For evaluation of useful heat energy gain by air passing through the duct for steady state condition can be used equation [3,6]

$$Q_u = A_c F_o \left[(\tau\alpha_a)_e - U_L(T_{fo} - T_{fi})\right] , \tag{1}$$

where F_o is the heat removal factor based on the outlet temperature of the air and is given by

$$F_o = \frac{GC_p}{U_L}\left[\exp\left(\frac{U_L F'}{GC_p}\right) - 1\right] . \tag{2}$$

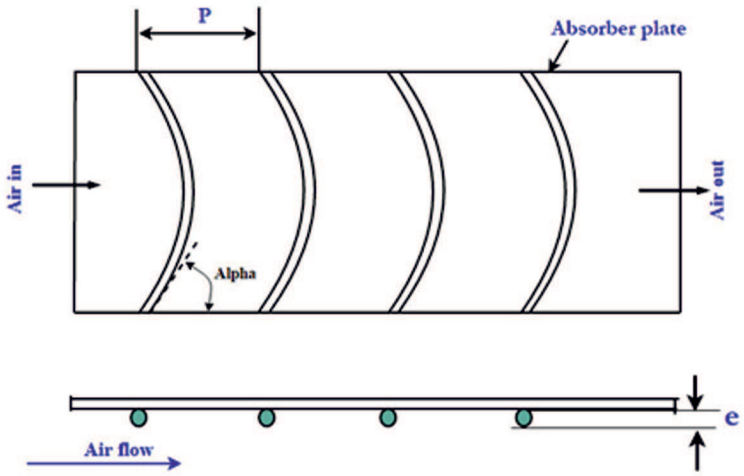

Figure 2: Geometry of wire rib roughness on the absorber plate.

Useful heat energy gain by air can also be given in terms of inlet and outlet air temperatures as

$$Q_u = \dot{m} C_p \left[T_{fo} - T_{fi} \right] \ . \tag{3}$$

The collector efficiency factor can be calculated as

$$F' = \frac{h_e}{h_e + U_L} \ , \tag{4}$$

where h_e is the equivalent heat transfer coefficient and can be given as

$$h_e = h_{c-ab-f} + \frac{h_{r-ab-bp} h_{c-bp-f}}{h_{r-ab-bp} + h_{c-bp-f}} \ . \tag{5}$$

The heat removal factor is evaluated by using the relationship

$$F_R = \frac{\dot{m} C_p}{U_L A_c} \left[1 - \exp\left(- \frac{U_L A_c F'}{\dot{m} C_p} \right) \right] = \frac{G C_p}{U_L} \left[1 - \exp\left(- \frac{U_L F'}{G C_p} \right) \right] \ , \tag{6}$$

where $G = \frac{\dot{m}}{A_c}$ is the mass flow rate per unit area of absorber plate surface.

The overall heat loss coefficient of the collector can be evaluated by the use of following equation [25]:

$$U_L = U_b + U_s + U_t \ . \tag{7}$$

The top loss coefficient (U_t) is a function of a number of parameters such as, absorber plate temperature, number of glass (glazing) covers, glazing temperature, etc. and is evaluated using an equation given in [1,3,4]. The Convective heat transfer coefficient (h_w) at the top glass cover due to wind (for $0 \leq V_w \leq 5$m/s) is given by [1,25]

$$h_w = 5.7 + 3.8V_w \ . \tag{8}$$

The bottom heat loss coefficient (U_b) and side heat loss coefficient (U_s) are respectively calculated using the following relations:

$$U_b = \frac{K_i}{\delta_i} \tag{9}$$

and

$$U_s = \frac{(L+W)t_e K_i}{LW\delta_i} \ . \tag{10}$$

The mean temperature of absorber plate can be given by [25]

$$T_{pm} = T_a + \left[\frac{Q_u}{A_c F_R U_L}\right](1 - F_R) \ . \tag{11}$$

The mean air temperature (T_{fm}) and mean bottom temperature (T_{bm}) can respectively be given as

$$T_{fm} = \frac{T_{fi} + T_{fo}}{2} = \frac{Q_u}{GA_c C_p} \tag{12}$$

and

$$T_{bm} = \frac{U_b T_a + T_{pm} h_{r-ab-bp} + h_{c-ab-f} T_{fm}}{U_b + h_{r-ab-bp} + h_{c-ab-f}} \ . \tag{13}$$

2.2 Evaluation of heat transfer coefficients

The radiative heat transfer coefficient between absorber plate and bottom plate can be calculated using the equation

$$h_{r-ab-bp} = \frac{\sigma(T_{pm}^2 + T_{bm}^2)(T_{pm} + T_{bm})}{\left(\frac{1}{\varepsilon_a} + \frac{1}{\varepsilon_b} - 1\right)} \ . \tag{14}$$

The convective heat transfer coefficient between glass cover and absorber plate due to natural convection is given by

$$h_{c-ab-c} = \frac{\mathrm{Nu}_c K_a}{L_1} \ , \tag{15}$$

where Nu_c is given by [1]

$$\mathrm{Nu}_c = 1 + 1.44\left[1 - \frac{1708}{\mathrm{Ra}\cos\beta}\right]^{+}\left[1 - \frac{1708(\sin 1.8\beta)^{1.6}}{\mathrm{Ra}\cos\beta}\right] + \left[\left(\frac{\mathrm{Ra}\cos\beta}{5830}\right)^{0.33} - 1\right]^{+} . \tag{16}$$

Here the '+' exponent implies that only positive values of the terms in the big brackets have to be considered and negative to be ignored. The above equation is valid for $0° \leq \beta \leq 75°$. The Rayleigh number can be obtained using the correlation

$$\mathrm{Ra} = \mathrm{GrPr} , \tag{17}$$

where, Grashof number (Gr) and Prandtl number (Pr) are respectively given by

$$\mathrm{Gr} = \left[\frac{g\beta'(T_{pm} - T_g)L_1^3}{\nu^2}\right] , \tag{18}$$

and

$$\mathrm{Pr} = \left[\frac{\mu C_p}{K_a}\right] . \tag{19}$$

The thermal expansion coefficient (β') of air in Eq. (18) is given by

$$\beta' = \left[\frac{1}{(0.5(T_{fo} + T_{fi}))}\right] . \tag{20}$$

For a duct having a smooth absorber plate and bottom plate the convective heat-transfer coefficients between flowing air and absorber plate (h_{c-ab-f}) as well as between flowing air and bottom plate (h_{c-bp-f}) are considered equal [25,26]. To calculate the heat-transfer coefficients h_{c-ab-f} and h_{c-bp-f} of a solar air heater duct with one side heated and remaining three sides properly insulated, the following correlation is used for turbulent flow ($\mathrm{Re} > 2300$) [25,26]:

$$h_{c-ab-f} = h_{c-bp-f} = \left[\mathrm{Nu}_s \frac{K_a}{D}\right] , \tag{21}$$

where the Nusselt number for a smooth duct is given by [27]

$$\mathrm{Nu}_s = 0.024\mathrm{Re}^{0.8}\mathrm{Pr}^{0.4} . \tag{22}$$

If the flow is laminar, then the following correlation for the case of parallel smooth plates with one plate at constant temperature and the other plate insulated [2] is used

$$\mathrm{Nu} = \left[\frac{h_{c-ab-f}D}{K_a}\right] = 4.9 + \frac{0.0606\left[\mathrm{RePr}\left(\frac{D}{L}\right)^{0.5}\right]}{1 + 0.0909\left[\mathrm{RePr}\left(\frac{D}{L}\right)^{0.7}\right]\mathrm{Pr}^{0.17}} \,. \tag{23}$$

The convective heat transfer coefficient between air and the wire rib-roughened absorber plate is calculated by using the equation

$$h_{c-ab-f} = \frac{\mathrm{Nu}_r K_a}{D} \,, \tag{24}$$

where the Nusselt number for rough surface is given by [27]

$$\mathrm{Nu}_r = 0.001047\mathrm{Re}^{1.3186}\left(\frac{e}{D}\right)^{0.3772}\left(\frac{\alpha}{90}\right)^{-0.1198} \,. \tag{25}$$

The hydraulic diameter for a duct of width (W) and depth (H) is calculated by

$$D = \frac{2WH}{(W+H)} \,. \tag{26}$$

Reynolds numbers is computed by using the following relationships:

$$\mathrm{Re} = \frac{2\dot{m}}{\mu(W+H)} \,. \tag{27}$$

2.3 Evaluation of friction factor and pressure drop

The friction factor for smooth plate solar air heater duct is evaluated by using the correlation given by [27]

$$f_s = 0.085\mathrm{Re}^{-0.25} \,. \tag{28}$$

The friction factor for arc shape wire roughened absorber plate of solar air heater duct, has been calculated by using the correlation [27]

$$f_r = 0.14408\mathrm{Re}^{-0.17103}\left(\frac{e}{D}\right)^{0.1765}\left(\frac{\alpha}{90}\right)^{0.1185} \,. \tag{29}$$

Accordingly, the drop of pressure in air heater duct can be calculated using the equation

$$\Delta p = \frac{4fLV^2\rho_a}{2D} \,. \tag{30}$$

2.4 Evaluation of exergy output rate

The true effect of a proposed augmentation technique on thermodynamic performance can be evaluated by comparing the irreversibility of the SAH duct before and after the implementation of the augmentation technique, i.e., by comparing the irreversibilities of conventional and artificially roughened SAH ducts. Considering a control volume of SAH, shown in Fig. 3 the exergy balance equation can be given as

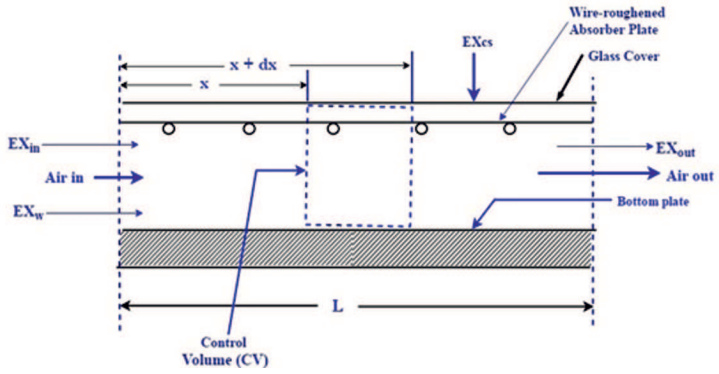

Figure 3: Control volume of exergy analysis of SAH.

$$\sum EX_{in} - \sum EX_{out} = IR \tag{31}$$

or

$$EX_i + EX_s + EX_w - EX_o = IR\,, \tag{32}$$

where EX_i is the exergy of air with mass flow entering the control volume (CV), EX_o is the exergy of air with mass flow rate leaving the control volume, $EX_s$is the exergy of solar radiation incident on glass cover, EX_w is the exergy of work input required to pump the air through the solar air heater and IR is the irreversibility or exergy loss of the air heating processes.

Equation (32) can be re-written in the form

$$IR = EX_s - [EX_o - EX_i - EX_w] \tag{33}$$

or

$$IR = EX_s - [EX_{u,p}]\,, \tag{34}$$

where $EX_{u,p}$ is the useful exergy gain including the blower work by air flowing through the SAH duct, and is given by

$$EX_{u,p} = EX_o - EX_i - EX_w = \\ = \dot{m}C_p(T_{fo} - T_{fi}) - \dot{m}C_pT_a \ln\left(\frac{T_{fo}}{T_{fi}}\right) - \frac{T_{fo}}{T_{fi}}\dot{W}_p \,. \tag{35}$$

The entropy created owing to heating of air and the blower work is

$$S_{gen} = \dot{m}C_p \ln\left(\frac{T_{fo}}{T_{fi}}\right) + \frac{\dot{W}_p}{T_{fi}} \,. \tag{36}$$

Total entropy generated is given by [28–30]

$$(S_{gen})_{Total} = T_a S_{gen} \,. \tag{37}$$

The blower work is calculated as

$$\dot{W}_p = \frac{\dot{m}\Delta p}{\eta_{pm}\rho_a} \,, \tag{38}$$

where η_{pm} is pump-motor efficiency and may be considered equal to 0.85 [5].

The exergy collection efficiency based on second law of thermodynamics by taking exergy of solar radiation can be written as [7,8]

$$\eta_{Ex} = \frac{EX_{u,p}}{EX_i} = \frac{EX_{u,p}}{A_c I\xi} \,, \tag{39}$$

where, ξ is the exergy efficiency of incident solar energy and is given by [24]

$$\xi = 1 - \frac{4}{3}\left(\frac{T_a}{T_s}\right) + \frac{1}{3}\left(\frac{T_a}{T_s}\right)^4 \tag{40}$$

and the sky temperature is given by [1]

$$T_s = 0.0552T_a^{1.5} \,. \tag{41}$$

In order to quantify the thermodynamic impact of an augmentation technique, a term called 'augmentation entropy generation number' (Na) is defined which is the ratio of entropy generation rate of augmented (or artificially roughened) surface to that of the smooth surface and is expressed by [23]

$$\mathrm{Na} = \frac{S_{gen,r}}{S_{gen,s}} = \left[\frac{\mathrm{St}_s(1+\kappa_r)}{\mathrm{St}_r(1+\kappa_s)}\right]\left(\frac{Q_{u_r}}{Q_{u_s}}\right) \,, \tag{42}$$

where abbreviation 's' stands for smooth absorber plate SAH and 'r' stands for roughened absorber plate SAH.

In Eq. (42) κ denotes the ratio of irreversibility distribution, defined as the ratio of fluid friction irreversibility to heat transfer irreversibility and can be given as

$$\kappa = 2\left(\frac{0.5f}{\mathrm{St}}\right)\left(1+\frac{H}{W}\right)\left(\frac{V^2}{C_pT_{fm}}\right)\left(\frac{T_{fm}}{\Delta T_{fm}}\right) , \tag{43}$$

where ΔT_{fm} is the bulk fluid (air) temperature difference. The Stanton number in Eq. (43) can be calculated by the equation

$$\mathrm{St} = \frac{\mathrm{Nu}}{\mathrm{RePr}} . \tag{44}$$

3 Numerical calculations

The useful heat energy output rate (Q_u), useful exergy output rate ($EX_{u,p}$), augmentation entropy generation number (Na) and entropy generation (S_{gen}) of wire roughened SAH for various mass flow rates and solar radiation intensities have numerically been calculated using collector configuration of Figs. 1 and 2. The values of system and operating parameters, as given in Tab. 1, have been used in the calculation.

In order to determine the various heat transfer coefficients h_{c-ab-f}, $h_{r-ab-bp}$, h_{c-bp-f}, h_{c-ab-c} and $h_{r-ab-bp}$, an initial guess value of mean plate temperature (T_{pm}), mean air temperature (T_{fm}) and mean bottom plate temperature (T_{bm}) are considered. With this initial values of T_{pm}, T_{fm}, and T_{bm} an initial approximate value of Q_u, F_R, F' are evaluated. Than the new temperatures of T_{pm}, T_{fm}, and T_{bm} are evaluated with Eqs. (11), (12) and (13), respectively. If the new calculated values differ by more than 0.01 °C from its previous initial assumed value, then this new temperatures are used as the initial temperature for the next iteration. The above process is kept continued till the final value of temperatures T_{pm}, T_{fm}, and T_{bm} are converged to a minimum deviation.

Finally, the converged values of T_{pm}, T_{fm}, and T_{bm} are used to obtain the energy output rate from Eq. (3), exergy output rate from Eq. (35), total entropy generation from Eq. (37) and Na from Eq. (42). To evaluate all above stated parameters numerically, programming codes have been developed in Matlab 2013 language and interactive environment.

Table 1: Range/base values of system and operating parameters used in the present investigation.

No	Parameters	Symbol	Units	Base value
Fixed System and Operating Parameters				
1	Duct length	L	m	1.5
2	Collector width	W	m	0.5
3	Rib pitch-to-height ratio, dimensionless	P/e	–	10
4	Roughness pitch	P	mm	20
5	Number of glass covers, dimensionless	M	–	1.0
6	Thermal conductivity of insulation	K_i	W/m K	0.037
7	Thermal conductivity of glass	K_g	W/m K	0.75
8	Thickness of insulation(	δ_i	m	0.05
9	Effective transmittance absorptance product	$(\tau\alpha_a)_e$	–	0.85
10	Emissivity of absorber plate, dimensionless	ε_P	–	0.9
11	Emissivity of bottom plate, dimensionless	ε_b	–	0.9
12	Emissivity of glass cover, dimensionless	ε_g	–	0.88
13	Thickness of glass cover	L_g	m	0.004
14	Air gap between absorber plate and glass cover	L_1	m	0.05
15	Atmospheric temperature	T_a	K	300
	Wind velocity	V_w	m/s	1.5
Variable Operating and System Parameters				
16	Rib height-to-duct hydraulic diameter ratio, dimensionless	$\frac{e}{D}$	–	0.021–0.042
17	Rib roughness height	e	mm	1–2
18	Duct depth	H	m	0.025–0.050
19	Flow-attack-angle, dimensionless	$\alpha/90$	–	0.33–0.66
20	Mass flow rate per unit area	G	kg/m^{2}h	10–550
21	Reynolds number	Re	–	450–21500
22	Intensity of solar radiation or insolation	I	W/m^2	800–1000

4 Results and discussion

4.1 Effects of mass flow rate and inlet air temperature on energy output rate and entropy created term

Figures 4a and 4b show the variations of energy output rate (Q_u) and entropy created term ($T_a S_{gen}$) with mass flow rate G for roughened absorber plate SAH. The fixed parameters, like solar radiation $I = 850$ W/m^2, surface area of collector plate $A_c = 0.75$ m^2, duct depth $H = 0.025$ m and inlet air temperature $T_{fi} = 300$ K (in Fig. 4a) and $T_{fi} = 335$ K (in

Fig.4b) respectively were taken. The values of roughness parameters like rib height-to-duct hydraulic diameter ratio (e/D), flow-attack-angle ($\alpha/90$) and rib pitch-to-height ratio (P/e) were taken fixed as 0.042, 0.33, and 10, respectively.

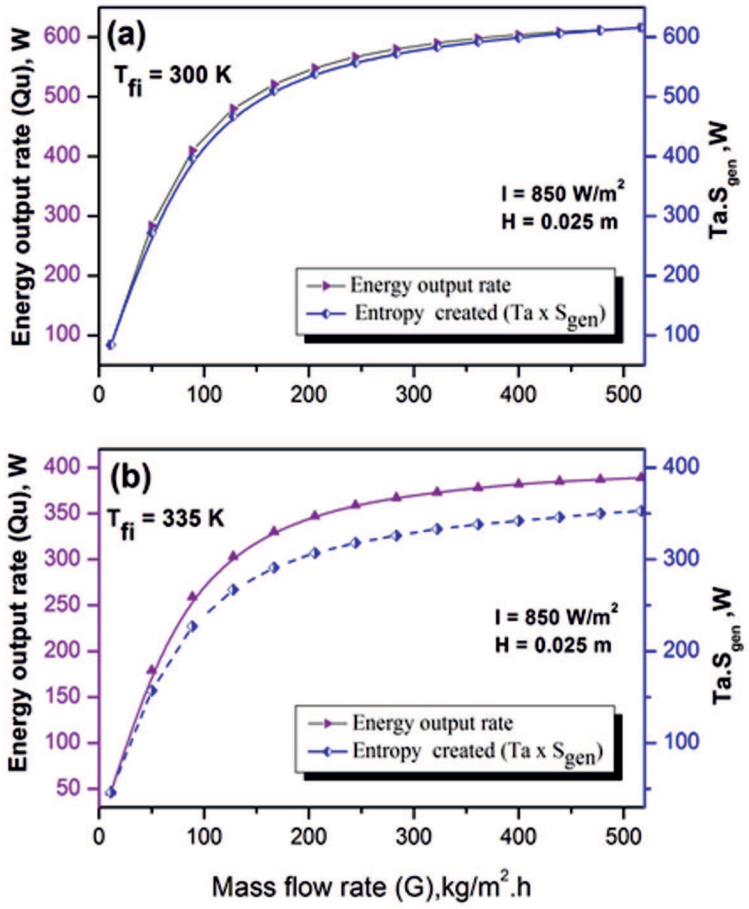

Figure 4: Variation of energy output rate (Q_u) and entropy created ($T_a S_{gen}$) with mass flow rate (G): (a) at $T_{fi} = 300$ K, (b) at $T_{fi} = 335$ K.

It is evident from these figures that, for both of the low and high temperatures of inlet air, energy output rate and entropy created term follow an increasing trend with increase in the mass flow rate. For low-value of inlet air temperature (300 K) in Fig. 4a, the numerical values of energy output rate and entropy created term is higher as compared to that at high inlet

air temperature (335 K) in Fig. 4b. For instance the numerical values of energy output rate Q_u = 548 W at mass flow rate G = 205 kg/m^{2}h and T_{fi} = 300 K, while at the same mass flow rate, Q_u= 347 W for a high value of inlet air temperature T_{fi} = 335 K have been recorded. Similarly, numerical values of entropy created term ($T_a S_{gen}$) is 607 W at mass flow rate G = 438 kg/m^{2}h and T_{fi} = 300 K while for the same mass flow rate is 346 W at T_{fi} = 335 K.

It can also be seen from Fig. 4a that energy output rate increases with mass flow rate and after certain value of mass flow rate it becomes almost equal to entropy created term and with further increase in the value of mass flow rate, the numerical values of $T_a S_{gen}$ is higher as compared to Q_u. Hence based on only the criteria of heat energy gain, operation of SAH at lower value of inlet air temperature is recommended for its enhanced performance.

4.2 Effects of mass flow rate and inlet air temperature on exergy output rate and energy output rate

Figures 5a and 5b show the variations of exergy output rate ($EX_{u,p}$) and energy output rate (Q_u) with mass flow rate (G) for fixed values of Insolation I = 850 W/m^2, surface area of absorber plate A_c = 0.75 m^2, duct depth H = 0.025 m for T_{fi} = 300 K and 335 K, respectively for the roughened SAH. The fixed values of roughness parameters were taken as e/D = 0.042, $\alpha/90$ = 0.33, P/e =10.

As seen from these figures exergy output rate ($EX_{u,p}$) increases with mass flow rate up to a peak value corresponding to G = 88 kg/m^{2}h and then descends. It becomes negative at higher rates of mass flow ($G >$ 500 kg/m^{2}h) for roughened SAH. It happens due to the fact that at higher values of mass flow rate, the requirement of power to run the blower increases and consequently pressure drop also increases in the solar air heater duct. On the other hand, energy output rate continues to increase as in Figs. 5a and 5b with increase in the mass flow rate for any value (lower or higher) of T_{fi}.

As the inlet air temperature (T_{fi}) increases from 300 K to 335 K, exergy peak, i.e., the point of highest value of exergy output rate shifts from 13.5 W, at mass flow rate of 88 kg/m^{2}h, (Fig. 5a) to 40.7 W, at mass flow rate of 283 kg/m^{2}h (Fig. 5b). So, for getting higher rate of exergy output at lower inlet air temperature, it is more rational to keep the mass flow rate in lower range as compared to that at higher range of inlet air temperature.

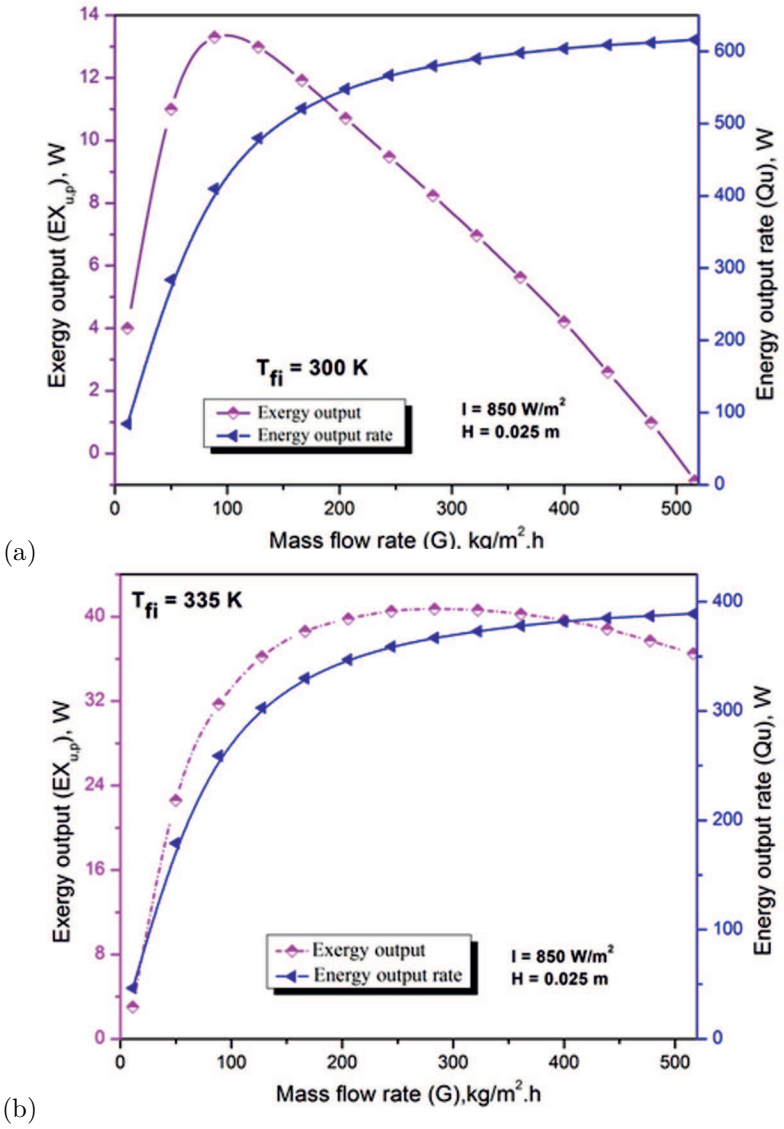

Figure 5: Variation of exergy output rate ($EX_{u,p}$)and energy output rate (Q_u) with mass flow rate (G) at (a) $T_{fi} = 300$ K, (b) $T_{fi} = 335$ K.

The variations of exergy output rate and energy output rate with mass flow rate and inlet air temperature, have been shown respectively in Figs. 6 and 7 for roughened SAH. The values of duct depth and collector plate

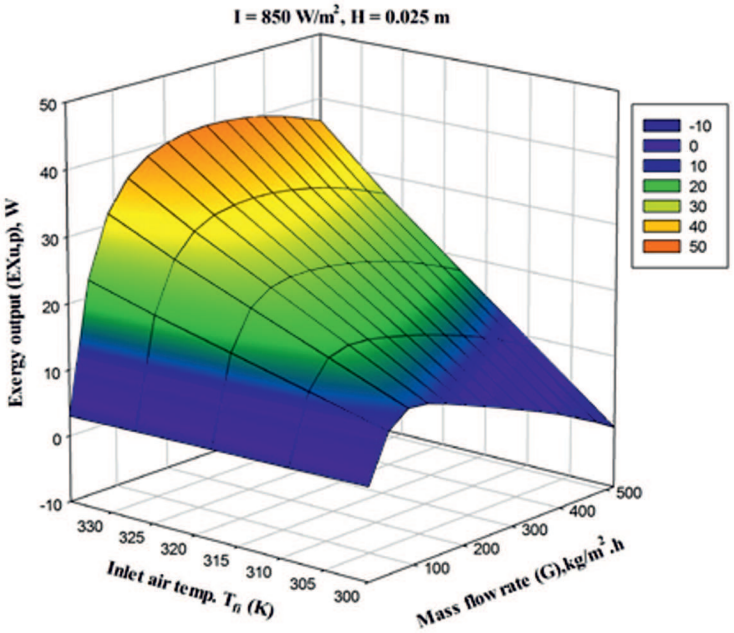

Figure 6: Variation of exergy output rate ($EX_{u,p}$) with mass flow rate (G) and inlet air temperature (T_{fi}).

area have been taken the same as in above case (Figs. 5a and 5b) while the inlet air temperatures have been varying from 300 K to 335 K.

It is evident from Fig. 6 that exergy output rate increases with mass flow rate up to a maximum value and after that it decreases, while it decreases with decrease in the value of inlet air temperature. The increase in exergy output rate with mass flow rate for any value of T_{fi} is not significant after a certain value of mass flow rate. So, it can be concluded from plot of Fig. 6, that there is a global optimum inlet air temperature for each values of mass flow rate that maximizes the exergy output for a given value of solar radiation intensity.

Furthermore, it can be seen from Fig. 7 that energy output rate is having continuous increasing trend with the mass flow rate, but its values decrease with increase of inlet air temperature values.

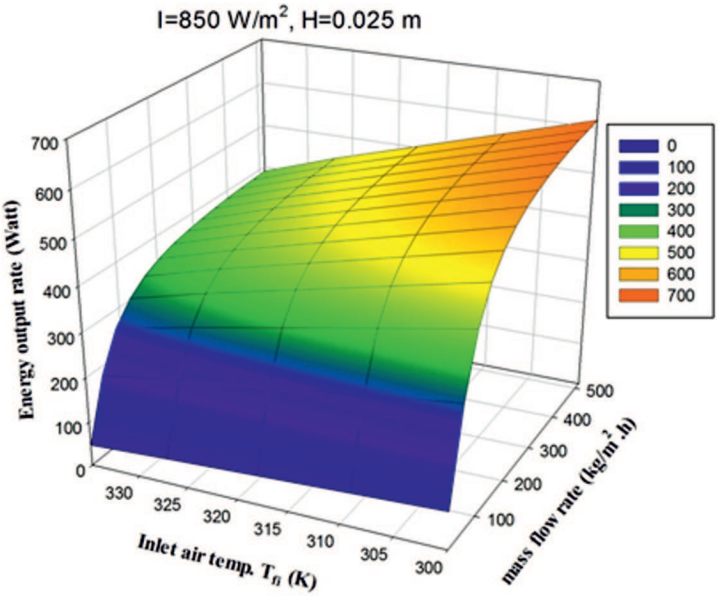

Figure 7: Variation of energy output rate (Q_u) with mass flow rate (G) and inlet air temperature (T_{fi}).

4.3 Effects of duct depths on exergy output rate as a function of mass flow rate

Figure 8 shows the variation of exergy output rate with mass flow rate (G) for various values of duct depths (H) ranging from 0.025 to 0.055 m and aspect ratio of collector duct (collector width- to-collector duct depth ratio) W/H = 9–20. It is evident from Fig. 8 that exergy output rate is the highest at lowest value of duct depth (H = 0.025 m). With increase in the value of H the peaks of exergy output rate fall down and shift towards higher mass flow rate of air. These results closely agree with the results presented by Sun *et al.* [31]. Furthermore, at lower values of mass flow rate (G) the exergy output rate is also high for lower values of H, but it decreases with faster rate with G and becomes negative at higher value of G. Thus, it can be concluded that for getting maximum exergy output rate, duct depth H should be low when the SAH operates in the lower range of mass flow rate.

The value of exergy output rate ($EX_{u,p}$) corresponding to $G = 280$ kg/m^{2}h is 8 W for the duct depth H = 0.025–0.035 m, as indicated by point 'a'

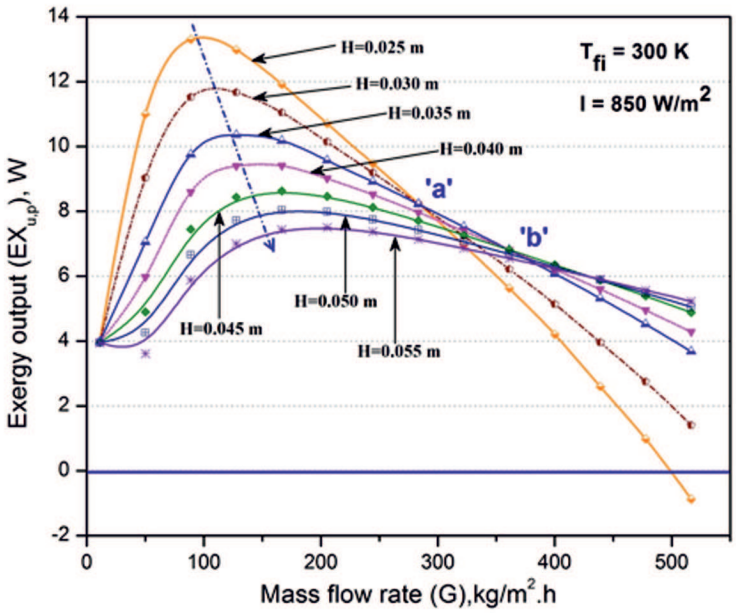

Figure 8: Variation of exergy output rate ($EX_{u,p}$) as a function of mass flow rate for different values of duct depth (H).

in Fig. 8, meaning that the variation in duct depth in this range does not affect $\mathrm{EX}_{u,p}$. Further it is also observed that the values of $EX_{u,p}$ converge at a point 'b' corresponding to mass flow rate $G = 375$ kg/m^{2}h for the duct depth in the range of 0.035–0.045 m and it is equal to 6.8 W. After this point 'b' $EX_{u,p}$ decreases with increase in G for all value of duct depth but with different rates which reveals that higher value of mass flow rate of air G beyond the limiting value ($G = 375$ kg/m^{2}h) is insignificant as far as exergetic performance of the arc shape wire rib roughened SAH is concerned.

4.4 Entropy generation minimization

Figures 9 and 10 show the variation of Na as a function of temperature rise parameter $(T_{fo}\text{-}T_{fi})/I$ for different values of e/D and $\alpha/90$, respectively. The values of other fixed parameters are shown in the figures. It can be seen from Fig. 9 that the Na decreases rapidly with increase in temperature rise parameter, reaches a minima for temperature rise parameter of about 0.0085 Km^2/W for $e/D = 0.042$ at $L = 1.5$ m, $W = 0.5$ m (i.e., $A_c =$

0.75 m^2), H = 0.025 m, and I = 850 W/m^2, and after that it increases steadily with further increase in $(T_{fo}\text{-}T_{fi})/I$. Similar trend of variation of Na with $(T_{fo}\text{-}T_{fi})/I$ for lower values of e/D is observed, but with different points of minimum Na. It can also be seen that entropy generation rate has almost same values up to temperature rise parameter of 0.006 Km^2/W for all values of e/D and after that all curves get separated and reaches its minima. Hence, it can be said that for individual curve there has a global minima of Na corresponding to geometrical, operating and temperature rise parameter. It can be concluded from Fig. 9 that Na decreases with the increase in e/D.

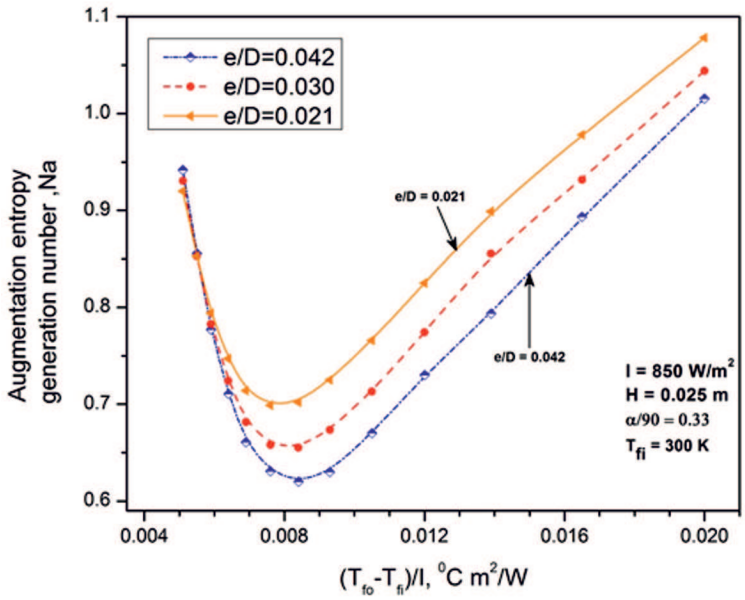

Figure 9: Variation of augmentation entropy generation number (Na) with temperature rise parameter $(T_{fo}\text{-}T_{fi})/I$ for different values of e/D.

Figure 10 shows the effect of different values of flow attack-angle $\alpha/90$ on the Na as function of temperature rise parameter. The entropy generation number has the lowest minimum value corresponding to $\alpha/90$=0.33, whereas it has the highest minimum value corresponding to $\alpha/90$=0.66. In the lower range of temperature rise parameter $(T_{fo} - T_{fi})/I < 0.0085\,Km^2/W$, there is a rapid fall in Na for all values *of* $\alpha/90$. The nature of variation of Na with $(T_{fo}\text{-}T_{fi})/I$ are similar for all values of $\alpha/90$.

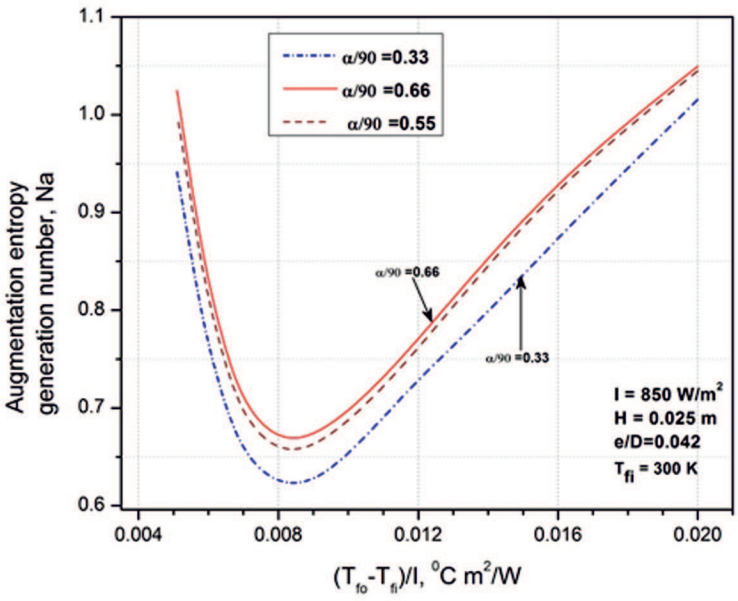

Figure 10: Variation of augmentation entropy generation number (Na) with temperature rise parameter $(T_{fo}\text{-}T_{fi})/I$ for different values of $\alpha/90$.

The values of different parameters like entropy created term (S_{gen}), total entropy generation ($T_a S_{gen}$), useful exergy output rate (EXu,p) and second law efficiency or exergy efficiency (η_{Ex}) with corresponding values of mass flow rates and Reynolds number, have been tabulated in Tab. 3 for the arc shape wire roughened SAH to see the simultaneous effects of the parameters at a glance. The geometrical, operating and rib roughness parameters used in the calculation have also been mentioned in the table.

4.5 Comparison of augmentation entropy generation number

Figure 11 shows the comparison of augmentation entropy generation numbers Na obtained in the present investigation with those obtained from SAHs having other roughness geometries, e.g., W-shape wire ribs [32], U-shape ribs [33], Inclined with gap wire ribs [34], continuous inclined wire ribs [35], and metal grit ribs [36] on the absorber plates for common roughness parameters and operating parameters, using the respective correlations, as given in Tab. 2.

A plot of Na as a function of $(T_{fo}\text{-}T_{fi})/I$, obtained for the SAHs having

Table 2: Heat transfer coefficient and friction factor correlations for solar air heater duct with different roughness elements on absorber plate.

Investigators	Roughness Geometry	Roughness & operating parameters	Heat transfer coefficient	Friction factor
Lanjewar *et al.* [32]	W-shape wire rib roughness	$e/D = 0.042$ $P/e = 10$ $\alpha = 60°$ $I = 850$ W/m^2 $H = 0.025$ m $T_{fi} = 300$ K	$\mathrm{Nu} = 0.0613\mathrm{Re}^{0.9079}(e/D)^{0.4487}$ $(\alpha/60)^{-0.1331}$ $\exp[-0.5307 \times (\ln(\alpha/60)^2]$	$f = 0.6182\mathrm{Re}^{-0.2254}(e/D)^{0.4622}$ $(\alpha/60)^{0.0817}$ $\exp[-0.28 \times (\ln(\alpha/60)^2]$
Bopche and Tandale [33]	U-shape ribs	$e/D = 0.042$ $P/e = 10$ $\alpha = 60°$ $I = 850$ W/m^2 $H = 0.025$ m $T_{fi} = 300$ K	$\mathrm{Nu} = 0.5429\mathrm{Re}^{0.7054}(e/D)^{0.3619}$ $(P/e)^{-0.1592}$	$f = 1.2134\mathrm{Re}^{-0.2376}(e/D)^{0.3285}$ $(P/e)^{-0.4259}$
Aharwal *et al.* [34]	Inclined wire rib with gap ribs	$e/D = 0.042$ $P/e = 10$ $\alpha = 60°$ $I = 850$ W/m^2 $H = 0.025$ m $g/e = 1$ $d/w = 0.25$ $T_{fi} = 300$ K	$\mathrm{Nu} = 0.012\mathrm{Re}^{1.148}(e/D)^{0.0104}$ $\left[\{1 - (0.25 - (d/w)^2(0.01(1 - g/e)^2\}\right]$	$f = 0.5\mathrm{Re}^{-0.0836}(e/D)^{0.72}$
Gupta *et al.* [35]	Inclined continious wire ribs	$e/D = 0.042$ $P/e = 10$ $\alpha = 60°$ $I = 850$ W/m^2 $W/H = 10$ $T_{fi} = 300$ K	$\mathrm{Nu} = 0.0024(e/D)^{0.001}(W/H)^{-0.06}$ $\mathrm{Re}^{1.084} \times \exp[-0.04(1 - \alpha/60)^2]$ For $\mathrm{Re}^+ \leq 35$ $\mathrm{Nu} = 0.0071(e/D)^{-0.24}(W/H)^{-0.028}$ $\mathrm{Re}^{0.88} \times \exp[-0.475(1 - \alpha/60)^2]$ For $\mathrm{Re}^+ \geq 35$	$f = 0.1911(e/D)^{0.196}(W/H)^{-0.093}$ $\mathrm{Re}^{-0.165} \times \exp[-0.0993(1 - \alpha/60)^2]$
Karmare and Tikekar [36]	Metal grit ribs	$e/D = 0.042$ $P/e = 10$ $l/s = 1.72$ $I = 850$ W/m^2 $H = 0.025$ m $T_{fi} = 300$ K	$\mathrm{Nu} = 2.4 \times 10^{-3} \times \mathrm{Re}^{1.3} \times (e/D)^{0.42}$ $(l/s)^{-0.146} \times (P/e)^{-0.27}$	$f = 15.55 \times \mathrm{Re}^{-0.263} \times (e/D)^{0.91}$ $(l/s)^{-0.27} \times (P/e)^{-0.51}$
Present study	Arc shaped wire rib roughness	$e/D = 0.042$ $P/e = 10$ $\alpha/90 = 0.33$ $I = 850$ W/m^2 $H = 0.025$ m $T_{fi} = 300$ K	$\mathrm{Nu} = 0.001047(\mathrm{Re})^{1.3186}(e/D)^{0.3772}$ $(\alpha/90)^{-0.1198}$	$f = 0.14408(\mathrm{Re})^{-0.17103}(e/D)^{0.1765}$ $(\alpha/90)^{0.1185}$

different roughness geometries on absorber plates [32-36], including the arc shape wire rib roughened absorber plate (present work) has been exhibited in Fig. 11. A similar plot, in the lower range of $(T_{fo}\text{-}T_{fi})/I = 0.004$–$0.010$ (Km^2)/W, but in enlarged view has been shown in Fig. 12 for better interpretation.

It is observed from Fig. 11 that the nature of variation of Na with $(T_{fo}\text{-}T_{fi})/I$ for arc shaped wire rib roughened SAH follows the similar pattern of variation to the SAHs of other roughness geometries on absorber plates [32–36] which validates the perfection of the results obtained by mathematical modelling of the system in the present work. It is observed from Figs. 11 and 12 that every roughened SAH is having higher values of Na as compared to the present roughened SAH for all values of $(T_{fo}\text{-}T_{fi})/I <$ 0.0085 Km^2/W. The SAHs with W-shape wire rib [32], U-shape rib [33], inclined rib with gap [34] exhibit the lower value of entropy generation

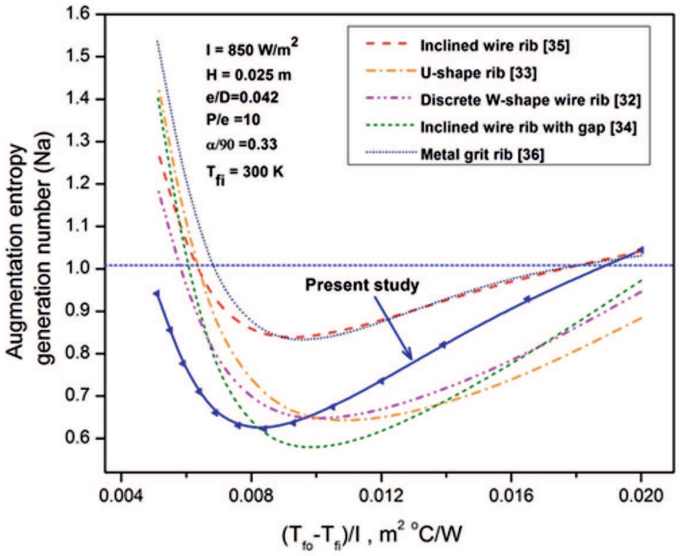

Figure 11: Comparison of augmentation entropy generation number (Na) of arc-shape wire roughness geometry with other roughness geometries of roughened SAH duct.

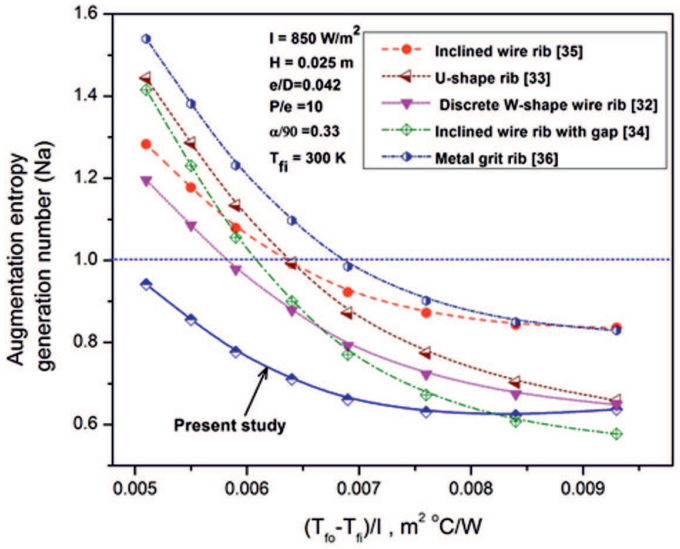

Figure 12: Comparison of augmentation entropy generation number (Na) of arc-shape wire roughness geometry with other roughness geometries of roughened SAH duct in lower range temperature rise parameter below 0.010 °C m^2/W.

Table 3: Results of entropy created, total entropy generation term, useful exergy output rate etc. of SAH with arc shaped wire roughness at $I = 850$ W/m^2, $W = 0.5$ m, $L = 1.5$ m, $H = 0.025$ m, and $T_a = 300$ K.

e/D	*α/90*	Mass flow rates (G), kg/m^{2}h	Reynolds number (Re)	Entropy created (S_{gen}), W	Total entropy created ($T_a S_{gen}$), W	Useful exergy output rate ($EX_{u,p}$), W	EX_i, W	Exergy efficiency (η_{Ex}), %
0.0420	0.33	11	453	0.70	211.11	4.02	4.19	0.95
		50	2038	0.80	242.04	11.0	4.19	2.62
		88	3624	1.21	365.76	13.3	4.19	3.17
		127	5210	1.46	440.55	12.98	4.19	3.09
		166	6796	1.62	487.17	11.92	4.19	2.84
		205	8381	1.72	518.97	10.71	4.19	2.55
		244	9967	1.80	541.5	9.48	4.19	2.26
		283	11553	1.86	558.21	8.24	4.19	1.96
		322	13139	1.90	571.05	6.96	4.19	1.66
		361	14725	1.93	581.25	5.63	4.19	1.34
		400	16310	1.96	589.53	4.21	4.19	1.00
		438	17896	1.98	596.49	2.6	4.19	0.62
		477	19482	2.00	602.52	0.98	4.19	0.23
		519	21068	2.02	607.74	-0.87	4.19	-0.20

number than arc shaped wire rib roughened SAH for temperature rise parameter $(T_{fo}\text{-}T_{fi})/I > 0.0085$ Km^2/W.

In order to quantify the thermodynamic impact of the different heat transfer enhancement techniques, i.e. of the different artificially roughened geometries on the absorber plates of SAHs the concept of Na is introduced. A heat enhancement system with Na < 1 is thermodynamically advantageous. The value showing Na $= 1$ has been marked by a horizontal line in Figs. 11 and 12. The values of Na lower than 1 correspond to a lower value of irreversibility of the system due to inclusion of roughness materials of different geometries on the absorber plate facing the air-flow side under the predefined conditions of geometrical, operating and air temperature rise parameters of the SAH.

5 Conclusions

This paper presents a parametric study to predict the energy output rate, exergy output rate, augmentation entropy generation number and entropy generation minimization of an arc shape wire rib roughened solar air heater (SAH). Based on the results the following conclusions are drawn.

1. With the increase in inlet air temperature energy output rate decreases, while the exergy output rate shows the reverse nature, i.e., with increase in inlet air temperature exergy output rate increases. Hence, based on the energy output rate evaluation criterion to obtain higher energy output rate for an arc shape wire rib roughened solar air heater it is recommended to operate the system at low inlet air temperature.
2. Exergy output rate increases with mass flow rate upto a certain value and then decreases. Furthermore, for each value of inlet air temperature there will be a global maximum value of mass flow rate, depending upon the range of system and operating parameters investigated.
3. The maximum exergy output rate is obtained in lower-range of mass flow rate at low inlet air temperature and at higher value of inlet air temperature maximum value of exergy-output rate is obtained in higher range of mass flow rate.
4. The high value of exergy output rate is obtained at highest value of aspect ratio of collector duct (with to depth, W/H) but only in the lower range of mass flow rate ($G < 100$ kg/m^{2}h).
5. The augmentation entropy generation number (Na) attains the value lower than 1, which is considered thermodynamically advantageous for every set of values of e/D and $\alpha/90$ corresponding to temperature rise parameter $\frac{\triangle T}{I} = 0.004\,\mathrm{Km}^2/\mathrm{W}$ to 0.010 Km^2/W. The lowest Na in the present investigation has been obtained at the set of roughness parameters: rib height-to-duct hydraulic diameter ratio $e/D = 0.042$, flow-attack-angle $\alpha/90 = 0.33$, and rib pitch-to-height ratio $P/e = 10$.
6. For $\frac{\triangle T}{I} < 0.0085\,\mathrm{Km}^2/\mathrm{W}$, the solar air heater with arc shape wire roughened absorber plate has lower value of Na than those of inclined wire rib, U-shape rib, discrete W-shape wire rib and metal grit rib roughened solar air heaters.

Received in 21 November 2017

References

[1] Duffie J.A., Beckman W.A.: *Solar Engineering of Thermal Processes*, 2nd Edn. John Wiley, New York 1991.

[2] Lanjewar A., Bhagoria J.L., Sarviya R.M.: *Experimental study of augmented heat transfer and friction in solar air heater with different orientations of W-Rib roughness*. Exp. Thermal Fluid Sci. **35**(2011), 986–995.

[3] Prasad R.K.: *Thermal performance characteristics of unidirectional flow porous bed solar energy collectors for heating air*. PhD thesis 1993 IIT, Roorkee.

[4] Sahu M.K., Prasad R.K.: *Investigation on optimal thermohydraulic performance of a solar air heater having arc shaped wire rib roughness on absorber plate*. Int. J. Thermodyn. **19**(2016), 4, 214–224, DOI: 10.5541/ijot.5000198432.

[5] Gawande V.B., Dhoble A.S., Zodpe D.B.: *Effect of roughness geometries on heat transfer enhancement in solar thermal systems – A review*. Renew. Sust. Energ. Rev. **32**(2014), 347–378.

[6] Singh S., Chander S., Saini J.S.: *Exergy based analysis of solar air heater having discrete V-down rib roughness on absorber plate*. Energy **37**(2012), 749–758.

[7] Chamoli S., Thakur N.S.: *Exergetic performance evaluation of solar air heater having V-down perforated baffles on the absorber plate*. J. Therm. Anal. Calorim. **117**(2014), 2, 909–923.

[8] Kazé C.V.A., Tchinda R.: *Exergy analysis of an air solar heater*. Int. J. Exergy. **11**(2012), 1, 19–34.

[9] Sciacovelli A., Verda V., Sciubba E.: *Entropy generation analysis as a design tool – A review*. Renew. Sust. Energ. Rev. **42**(2015), 1167–1181.

[10] Hepbasli A.: *A key review on exergetic analysis and assessment of renewable energy resources for sustainable future*. Renew. Sust. Energ. Rev. **12**(2008), 593–661.

[11] Saidur R., Boroumand Jazi G., Mekhlif S., Jameel M.: *Exergy analysis of solar energy applications*. Renew. Sust. Energ. Rev. **16**(2012), 350–356.

[12] Bejan A.: *A study of entropy generation in fundamental convective heat transfer*. J. Heat Trans. **101**(1979), 718-725.

[13] Bejan A.: *The concept of irreversibility in heat exchanger design: counter flow heat exchangers for gas–to-gas applications*. J. Heat Trans. **99**(1977), 374–380.

[14] Nag P.K., Mukherjee P.: *Thermodynamic optimization of convective heat transfer through a duct with constant wall temperature*. Int. J. Heat Mass Tran. **30**(1987), 401–405.

[15] Ko T.H., Ting K.: *Entropy generation and optimal analysis for laminar forced convective in curved rectangular ducts: a numerical study*. Int. J. Therm. Sci. **45**(2006), 138–150.

[16] Ko T.H.: *Numerical analysis of entropy generation and optimal Reynolds number for developing laminar forced convection in double-sine ducts with various aspect ratios*. Int. J. Heat Mass Tran. **49**(2006), 718–26.

[17] Yilbas B.S., Shuja S.Z., Budair M.O.: *Second law analysis of a swirling flow in a circular duct with restriction.* Int. J. Heat Mass Tran. **42**(1999), 4027–4041.

[18] Altfeld K., Leiner W., Fiebg M.: *Second law optimization of flat plate solar air heaters.* Solar Energy **41**(1988), 309–317.

[19] Sahiti N., Krasniqi F., Fejzullahu Xh., Bunjaku J., Muriqi A.: *Entropy generation minimization of a double-pipe pin fin heat exchanger.* Appl. Therm. Eng. **28**(2008), 2337–2344.

[20] Bejan A.: *Fundamental of exergy analysis, entropy generation minimization, and the generation of flow architecture.* Int. J. Energ. Res. **26**(2002), 545, DOI: 10.1002/er.804

[21] Ratts E.B., Raut A.G.: *Entropy generation minimization of fully developed internal flow with constant heat flux.* J. Heat Trans. **126**(2004), 656-659.

[22] Zhou Y.Y., Zhu L., Yu J.L, Li Y.Z.: *Optimization of plate fin heat exchanger by minimizing specific entropy generation rate.* Int. J. Heat Mass Tran. **78**(2014), 942–946.

[23] Layek A., Saini J.S., Solanki S.C.: *Second law optimization of a solar air heater having chamfered rib-groove roughness on absorber plate.* Renew. Energ. **32**(2007), 1967–80.

[24] Hedayatizadeh M., Yahya A., Sarhaddi F., Farahat S., Safavinejad A., Chaji H.: *Analysis of exergy and parametric study of a v-corrugated solar air heater.* Heat Mass Transfer **48**(2012), 1089–1101.

[25] Gupta M.K, Kaushik S.C.: *Performance evaluation of solar air heater having expanded metal mesh as artificial roughness on absorber plate.* Int. J. Therm. Sci. **48**(2009), 1007–1016.

[26] Tao L., Wenxian Lin: *A Parametric Study on the Thermal Performance of a solar air collector with a V-Groove absorber.* Int. J. Green Energy **4**(2007), 601–622.

[27] Saini S.K, Saini R.P.: *Development of correlations for Nusselt number and friction factor for solar air heater with roughened duct having arc-shaped wire as artificial roughness.* Solar Energy **82**(2008), 1118–1130.

[28] Keenan J.H.: *Availability and irreversibility in thermodynamics.* Br. J. Appl. Phys. **2**(1951), 183–192.

[29] Guoy G.: *Surlenergie utilizable (on usable energy).* J. Physics **11**(1889), 8, 501–518.

[30] Stodola A.: *Die Kreisprozesse der Gasmaschine (gas engine cycles).* Z Ver Dtsch Ing **32**(1898), 1086–1091.

[31] Wei Sun, Jie Ji, Wei He: *Influence of channel depth on the performance of solar air heaters.* Energy **35**(2010), 4201–4207.

[32] Lanjewar A., Bhagoria J.L., Sarviya R.M.: *Heat transfer and friction in solar air heater duct with W-shaped rib roughness on absorber plate.* Energy **36**(2011), 4531–4541.

[33] Bopche S.B, Tandale M.S.: *Experimental investigations on heat transfer and frictional characteristics of a turbulator roughened solar air heater duct.* Int. J. Heat Mass Tran. **52**(2009), 2834–2848.

[34] Aharwal K.R., Gandhi B.K., Saini J.S.: *Experimental investigation on heat-transfer enhancement due to a gap in an inclined continuous rib arrangement in a rectangular duct of solar air heater*. Renew. Energ. **33**(2008), 585–596.

[35] Gupta D., Solanki S.C., Saini J.S.: *Thermohydraulic performance of solar air heaters with roughened absorber plates*. Solar Energy **61**(1997), 33–42.

[36] Karmare S.V., Tikekar A.N.: *Heat transfer and friction factor correlation for artificially roughened duct with metal grit ribs*. Int. J. Heat Mass Tran. **50**(2007), 4342–51.